Carbon 186 (2022) 344–354

Contents lists available at ScienceDirect

Carbon

journal homepage: www.elsevier.com/locate/carbon

Research Paper

Liquid-phase water isotope separation using graphene-oxide membranes

Karin Ching [a], Andy Baker [b], Ryoji Tanaka [c], Tingwen Zhao [a], Zhen Su [a], Rodney S. Ruoff [d, e, **], Chuan Zhao [a, ***], Xianjue Chen [a, f, *]

[a] School of Chemistry, The University of New South Wales, Sydney, New South Wales, 2052, Australia
[b] School of Biological, Earth and Environmental Sciences, The University of New South Wales, Sydney, New South Wales, 2052, Australia
[c] The Pheasant Memorial Laboratory for Geochemistry and Cosmochemistry, Institute for Planetary Materials, Okayama University, Misasa, Tottori, 682-0193, Japan
[d] Center for Multidimensional Carbon Materials (CMCM), Institute for Basic Science (IBS), Ulsan, 44919, Republic of Korea
[e] Department of Chemistry, Department of Materials Science and Engineering, School of Energy and Chemical Engineering, Ulsan National Institute of Science and Technology (UNIST), Ulsan, 44919, Republic of Korea
[f] School of Environmental and Life Sciences, The University of Newcastle, Callaghan, New South Wales, 2308, Australia

ARTICLE INFO

Article history:
Received 4 August 2021
Received in revised form
20 September 2021
Accepted 2 October 2021
Available online 6 October 2021

Keywords:
Graphene oxide
Membranes
Water isotopes
Filtration
Isotope effect
Diffusion

ABSTRACT

We report pressure-driven liquid-phase isotope separation (dead-end filtration) to enrich D and ^{18}O in natural water using graphene oxide (G-O) and UV-reduced graphene oxide (UV-rG-O) membranes. The isotope diffusivity (*molecular diffusion* and *adsorption separation*) was found to be responsible for isotope separation. *Adsorption separation* is the dominant mechanism for improvements in D and ^{18}O enrichment via increased G-O loading that leads to the increased number of adsorption sites (epoxy and hydroxyl groups on G-O), and higher degrees of reduction of G-O that result in the narrowing of the nanochannels which decreases the portion of water molecules experiencing molecular diffusion. The best performing membrane was "UV-rG-O" made by exposing a G-O membrane to 24 h UV irradiation from one side, showing enrichment of D of 0.5% for D/H and ^{18}O of 0.08% for $^{18}O/^{16}O$ in a single-stage experiment, without contribution from the vapor pressure isotope effect. This work improves the understanding of the mechanisms for graphene-based membrane separation of D and ^{18}O enriched water.

1. Introduction

In natural water there are three naturally occurring isotopes for oxygen, oxygen-16 (^{16}O), oxygen-17 (^{17}O) and oxygen-18 (^{18}O), and for hydrogen, hydrogen-1 (^{1}H = H), hydrogen-2/deuterium (^{2}H = D) and hydrogen-3/tritium (^{3}H). ^{18}O and D are stable isotopes that are widely used. For example, ^{18}O is an essential precursor in the production of fluoride-18 for position emission tomography (PET) scans that are used in the diagnosis and management of cancer patients [1]. Heavy water (D_2O) is used as a moderator in nuclear reactors that generate carbon-free electricity and valuable radioisotopes for medicine and industry [2]. Additionally, D_2O and $H_2^{18}O$ are important tracers used in isotopic analysis and environmental studies [3]. Current techniques for enriching ^{18}O include cryogenic distillation of water and CO [4], oxygen gas, or NO gas [5]; or fractional distillation of water [6], and D enrichment can be achieved with chemical exchange (Girdler Sulfide Process), electrolysis, water distillation, and cryogenic distillation of hydrogen [7,8].

The separation of water molecules by differences in their isotope content arises from the differences in mass or mass distribution caused by D or ^{18}O substitution. In membrane-based water isotope separation, water molecules form hydrogen-bonds with neighboring water molecules and H-bonding functional groups on the

Abbreviations: G-O, graphene oxide; UV-rG-O, UV-reduced graphene oxide; MCE, mixed cellulose ester; X mL G-O, ('X' represents volume of graphene oxide solution) used to prepare graphene oxide films; Y h UV-rG-O, (Y represents the duration of UV exposure) used to prepared UV reduced graphene oxide films; ZPE, zero-point energy.

* School of Chemistry, The University of New South Wales, Sydney, New South Wales, 2052, Australia.
** Corresponding author. Center for Multidimensional Carbon Materials (CMCM), Institute for Basic Science (IBS), Ulsan, 44919, Republic of Korea.
*** Corresponding author.
E-mail addresses: ruofflab@gmail.com (R.S. Ruoff), chuan.zhao@unsw.edu.au (C. Zhao), sam.chen@newcastle.edu.au (X. Chen).

https://doi.org/10.1016/j.carbon.2021.10.009
0008-6223/

membrane. The difference in strength/length of the hydrogen bond are reported as one of the reasons behind isotope separation based on different rates of diffusion and selective absorption and desorption. Hydrogen-bond strength is influenced by the nuclear quantum effects, such as zero-point energy (ZPE) [9]. ZPE is related to the mass ratio of the two isotopes, H/D and $^{16}O/^{18}O$. The difference in ZPE between $H_2^{16}O$ and $D_2^{16}O$ is larger than that between $H_2^{16}O$ and $H_2^{18}O$ due to the larger change in mass ratio when substituting H with D compared to ^{16}O with ^{18}O [10]. The isotope effect experienced when substituting H with D is greater due to the change in the hydrogen-bond structure. Substitution with hydrogen or oxygen isotopes also affect the mass distribution of the water molecule. For H-bonded water molecules, it has been reported the average moment of inertia for $D_2^{16}O$ is larger than those of both $H_2^{16}O$ and $H_2^{18}O$ (and that of $H_2^{18}O$ is only slightly larger than that of H_2O) [9,11]. A larger moment of inertia lowers the frequency of hindered rotation, resulting in less energy stored at zero-point motions. Therefore, larger activation energies are required for breaking the H-bonding of deuterated water molecules [12]. These differences in diffusion and interactions with water and the functional groups on the membrane could lead to selective separation of water isotopes.

Membrane-based separation has been investigated as an alternative (e.g., to try to reduce costs and to try to simplify the process), particularly pervaporation and membrane distillation that have shown enhanced isotope separation with lower energy consumption due to the combined *vapor pressure effect*, *diffusion effect* and *selective adsorption* [13]. Chmieleswski et al. reported that for water vaporizing inside the pores of the membrane [14], the vapor pressure effect is largely responsible for D separation from H and the diffusion effect is mostly responsible for ^{18}O separation from ^{16}O [15]. Due to the reported relatively large ^{18}O separation from ^{16}O achieved with membrane distillation, researchers have directed their attention into improving the efficiency of this process [16,17] and producing hydrophobic, polymer based-membranes to enhance isotopic water separation [18].

In recent years, isotope separation has been reported for D at room temperature with membranes made of graphene, MoS_2, or *h*BN [19,20], and more recently for oxygen gas via cryogenic nanoporous adsorption at 112 K via “carbide-derived carbons” (CDC's) packed into columns [21]. The separation using the membranes is reported to be due to the “quantum sieving effect” induced by their nanoscale pore sizes. On the other hand, CDC's selective adsorption of $^{18}O_2$ is reported to be due to the “collective-nuclear-quantum effect” resulting from densely packed molecules in sub-nanometer pores at a low temperature. The permeation of water vapor through stacked graphene oxide layers was reported by Boehm et al., in 1961 [22]. More recently, it has been again reported that water can readily permeate through membranes comprised of stacked and overlapped G-O sheets [23]. Selective separations of ions and molecules through membranes composed of G-O or chemically modified G-O sheets are also reported to be possible due to charge and size-exclusion [24], and preferential adsorption [25].

There have been studies of G-O membranes for water isotope separation using vapor and liquid-vapor permeation for enriching D in water [26–29]. It has been reported that large sheet sizes, hydrophobicity, narrowed interlayer spacing and nanochannel uniformity are factors to improve D/H separation. However, the separation of isotopic water vapor is overshadowed by the vapor pressure isotope effect. For example, the separation factors reported for unmodified G-O membranes in air-gap membrane distillation ($\alpha = 1.044–1.055$) are below the vapor pressure isotope effect ($\alpha = 1.060$) at 40–45 °C [28,29]. Therefore, the contribution of G-O membranes to isotope separation is unclear as the reported enrichment is counteracted by a mixed ultrafiltration process in which liquid can permeate into the hydrophilic nanochannels of G-O [13,28]. Adjustments made to the surface hydrophobicity of G-O membranes via reduction, functionalization or coating have been studied for enhancing D/H separation [28,29], although these modifications made it harder to isolate the effect G-O has on isotope separation and the mechanism behind D enrichment in water. Furthermore, to the best of our knowledge, there have been no studies of G-O membranes for the enrichment of ^{18}O in water.

The reported mechanisms behind separation for liquid-phase permeation are molecular diffusion and selective adsorption. Molecular diffusion is described to occur within the nanochannels of the membrane where molecules collide with each other without interacting with the surface of the membrane [30]. It has been reported that in liquid-phase, molecular diffusion rates are dependent on the intermolecular interactions (intermolecular hydrogen bonds with neighboring water molecules) and, less significantly, the difference in molecular mass [31]. Generally, lighter isotopic molecules are reported to have a higher diffusion rate. On the other hand, selective adsorption is dependent on the bond strength formed between the isotopes and the adsorption sites, which results in the difference in adsorption enthalpies and desorption activation energies. Studies show that the affinity strength of the adsorption site is influenced by the ZPE of the isotopes and that heavier isotopes with a lower ZPE generally lead to preferential adsorption and slower desorption [8,12]. Studies have shown that $H_2^{18}O$ and D_2O form stronger hydrogen bonds with oxygen functional groups in cellulose membranes or on G-O [14,32]. The difference in adsorption strength of water molecules could affect their surface diffusion on G-O depending on adsorption and desorption rates. Heavier isotopes typically have a slower surface diffusion rate, although the opposite has been reported for activated carbon [33].

In this study, membranes of different G-O loadings were prepared to alter the thickness of the membranes and the number of adsorption sites. G-O membranes were also reduced with different degrees of reduction that altered the number of adsorption sites, surface hydrophobicity and d-spacing [34,35]. UV irradiation (365 nm) was selected for partial “reduction” (literally: deoxygenation) of G-O and the degree of deoxygenation can be controlled through exposure times. Unlike the chemically reduced G-O (rG-O) films, e.g., produced using hydrazine or hydroiodic acid and that are typically impermeable to water, the UV-reduced G-O (UV-rG-O) membranes remained permeable to water. Studies have shown that exposing G-O films to UV irradiation reduces the exposed G-O surface [34] and affects the water permeability of G-O membranes [35]. We have investigated the isotope effect that G-O and UV-rG-O membranes have on enriching D and ^{18}O in natural water by pressure-driven liquid-phase permeation (dead-end filtration) that minimizes the vaporization process. This study provides a better understanding of the mechanisms behind isotope separation and the membrane properties such as thickness, d-spacing and the surface chemistry of G-O sheets that are desirable for D/H and $^{18}O/^{16}O$ separation.

2. Experimental section

2.1. Membrane preparation

G-O was synthesized by exfoliating graphite oxide following the modified Hummers method, then G-O was dispersed in water at a concentration of 0.5 mg mL^{-1} [36,37]. G-O membranes were prepared by vacuum filtrating specific volumes (1, 3, or 5 mL) of the G-O dispersion through mixed cellulose ester (MCE) filters (Whatman™, 10401712, 0.2-μm pore size, 47-mm diameter) and dried in

air (named "1, 3, and 5 mL G-O"). For UV-rG-O membranes, dried G-O films prepared from 3 mL of the G-O dispersion on MCE filters were exposed to specific durations (3, 6 and 24 h) of UV (365 nm) radiation in the UVP Cl-1000L UV crosslinker (~3 mW cm^{-2}) at room temperature (named "0, 3, 6 and 24 h UV-rG-O"). The films were placed 12.5 cm below the 8 W UV lamps. All films were left on the MCE substrate and sandwiched with waterproof tape (Clear Gorilla Tape) for an effective area of 4.91 cm^2 and used as membranes for dead-end filtration (Fig. S1). To separate the MCE filter from the films for characterization, the film was thoroughly washed with acetone (Chem-Supply) to dissolve and remove the MCE filter.

2.2. Permeance of membranes

Dead-end filtration was carried out using stirred cells (Amicon®, 50 mL) connected to a manifold with a pressure chamber that supplies 1.0 bar of pressure using N_2 gas (Figs. S1b and c). 20.0 mL of water (feed) directly from the Milli-Q integral water purification system (Merck Millipore, USA) that achieves a water quality of ultrapure (ASTM Type 1, 18.2 MΩ cm at 25 °C, TOC <10 ppb) was added into the stirred cell. The feed (control) has a mixture of hydrogen and oxygen isotopes. 18.0 mL of water (permeate) passed through the membrane before the pressure was released, leaving the remaining water (retentate) in the stirred cell. For each membrane, dead-end filtration was carried out 3 times using a new membrane each time. The permeance (L m^{-2} h^{-1} bar^{-1}) was calculated according to the following equation.

$$Permeance = \frac{V_p}{A \cdot \Delta t \cdot P} \quad (1)$$

where V_p (L) is the volume of the permeate, A (m^2) is the effective area, Δt is the total time and P (bar) is the pressure applied.

The mass of the feed, permeate and retentate were recorded. Due to the low permeance of some of the membranes, mass loss from water evaporation were detected. To verify if the membrane component causes isotope separation beyond vapor phase change, control experiments were performed by replacing the G-O membrane with a copper foil sandwiched between waterproof tape as an impenetrable barrier. Additionally, Rayleigh's equation for fractional distillation [38] were used with the fractionation factor calculated from Horita et al.'s equation for liquid to vapor phase change [39] (see Supporting Information for control experiments and calculation details).

2.3. Separation performance of membranes

Water samples from the feed, permeate and retentate were collected and tested using the Laos Gatos Research (LGR) Isotopic Water Analyzer in liquid water mode (LGR LWIA, IWA-35EP) to determine the D/H and $^{18}O/^{16}O$, which are expressed in δ notation relative to VSMOW (Vienna Standard Mean Ocean Water) as,

$$\delta D \text{ or } \delta^{18}O = \frac{R_{sample}}{R_{VSMOW}} - 1 \quad (2)$$

where R is the isotope ratio for D/H or $^{18}O/^{16}O$ with the subscripts referring to the tested sample or the known isotope ratios in VSMOW given by the reference sheet [40]. All measurements were made using five commercially available working standards, LGR 1–5 (Ecotech) with known isotopic composition (δD, $\delta^{18}O$) of (−165.70‰, 21.28‰), (−123.80‰, −16.71‰), (−79.60‰, −11.04‰), (−49.20‰, −7.81‰) and (−9.90‰, −2.99‰), and a stable isotope international standard, Vienna Standard Mean Ocean Water 2 (VSMOW2, International Atomic Energy Agency (IAEA)) with known isotopic composition (δD, $\delta^{18}O$) of (0.00‰, 0.00‰), to cover the entire range of our sample measurements. The standards were analyzed routinely as references between every 15 water samples to check the instrument performance. The measured δD and $\delta^{18}O$ values for standards during the analytical sequences are <1.0‰ and <0.13‰, respectively, from the certified values. Each sample was run twice with 3 lead injections and 5 repeats which were averaged to determine δD and $\delta^{18}O$ values. From the isotope ratio, the separation factor for D and ^{18}O are determined using,

$$\alpha = \frac{R_R}{R_P} \quad (3)$$

where R is the isotope ratio for D/H or $^{18}O/^{16}O$ with the subscripts R and P referring to the retentate and permeate, respectively. The separation factor reported is the average of the separation factors from the water samples produced by three individual experiments using a new membrane each time. The error bars shown represent one standard deviation.

It should be noted that proton exchange between isotopic water molecules occurs, $H_2O + D_2O \rightleftharpoons 2HOD$ [14,41]. In the separation process, both HOD and D_2O will be enriched as increasing the D/H in water will increase the likelihood for D_2O to form, although, at low concentrations, HOD will be more common [42]. On the other hand, $H_2^{18}O$ is enriched with an increase in $^{18}O/^{16}O$ as no "exchange" of O happens in water.

The observed mass loss after dead-end filtration indicates the contribution of water evaporation to the enrichment of D and ^{18}O in the water samples. The isotope enrichment solely caused by the membrane was determined by subtracting the evaporative fractionation (calculated from Rayleigh's model [38] and Horita et al.'s equation [39], Eqs. (S1–S3)) from the percentage increase in the isotopic ratios measured from the control and enriched water sample in dead-end filtration. The change of D/H or $^{18}O/^{16}O$ as a percentage from dead-end filtration or Rayleigh's fractionation, was calculated by the equation below.

$$\Delta R = \left(\frac{R_{Enriched} - R_{Initial}}{R_{Initial}} \right) \quad (4)$$

where R is the isotope ratio for D/H or $^{18}O/^{16}O$ and the subscripts *Enriched* refers to the retentate from the dead-end filtration or the water sample after vaporization. The subscript *Initial* refers to the feed from the dead-end filtration or the water sample before vaporization.

2.4. Material characterization

Scanning electron microscopy (SEM) images were obtained on a FEI Nova NanoSEM 450 FE-SEM. Contact angle measurements were captured using a Rame-Hart goniometer. X-ray diffraction (XRD) patterns were obtained using an Empyrean Thin-Film XRD unit and analyzed using X'Pert HighScore Plus software. Raman spectra were recorded on a Renishaw InVia 2 Raman spectrometer at room temperature with a 532 nm laser excitation. X-ray photoelectron spectroscopy (XPS) spectra were acquired using an ESCALAB 250 Xi, Thermo Scientific. Depth profiles using time-of-flight secondary ion mass spectrometry (ToF-SIMS) were conducted on ION-TOF TOF.-SIMS 5. Analysis conducted used negative polarity by Bi^+ at 30 keV and sputtered with Cs^+ beam of 1 keV. Samples were prepared on silicon wafers with tape fixing the thin film except for the 24 h UV-rG-O which was directly placed onto the silicon wafer. The unexposed side of the membrane was attached facing up to allow the distinction of the interface between the reduced side of the film and the silicon wafer/tape.

3. Results and discussion

3.1. Characterization of membranes

G-O films were prepared by vacuum filtrating 1, 3 and 5 mL of 0.5 mg mL^{-1} G-O solution and the UV-rG-O films were prepared using 3 mL G-O films exposed to different durations of UV radiation with a wavelength of 365 nm which is reported to have sufficient energy to excite electrons in the sp^2 domains of G-O and generate electron-hole pairs [34,43,44]. It has been reported that the generated electron-hole pairs can reduce G-O by removing more reactive epoxy and hydroxyl groups on the basal plane [45]. The resulting UV exposed films remained intact with the color of the membrane progressively becoming darker, with the 24 h UV-rG-O possessing a dim sheen on the surface (Fig. S2b). These observations indicate that UV irradiation partially reduced the G-O films. Fig. 1 a and b show the thickness of the G-O and UV-rG-O membranes determined from the SEM cross sections shown in Fig. 1 c to h. The average film thickness increased with higher G-O loading, from 250, 490 to 730 nm for 1, 3 and 5 mL, respectively. Here a low light intensity, ~3 mW cm^{-2}, was used to minimize the expansion of the film. UV exposure of 490-nm-thick, 3 mL G-O resulted in minor changes to the film thickness, from 550 nm for 3 h UV exposure to 490 nm for 24 h UV exposure, and their lamellar structures remained intact. This suggests the G-O films did not experience rapid decomposition which has been reported to cause expansion [34,35] or large gaps in UV-rG-O films due to the release of CO, CO_2, and H_2O gas molecules [43].

Water contact angle measurements were carried out on the UV exposed surfaces, Fig. 1i. The pristine G-O surface had a water contact angle of 48°, and a similar contact angle was observed after 3 h UV exposure. Longer durations of UV irradiation increased water contact angle to 60° for 6 h UV exposure and to 62° for 24 h UV exposure. The higher water contact angle indicates an increased surface hydrophobicity, which can be owed to the removal of hydrophilic oxygen containing functional groups. This is consistent with the XPS and ToF-SIMS results discussed below.

Thin-film XRD patterns of the G-O and UV-rG-O films before (dry) and after soaking in water for 1 h (wet) are shown in Fig. 1j. The (001) peak of the G-O film shifts from 10.2° to 11.2°, 11.3° and

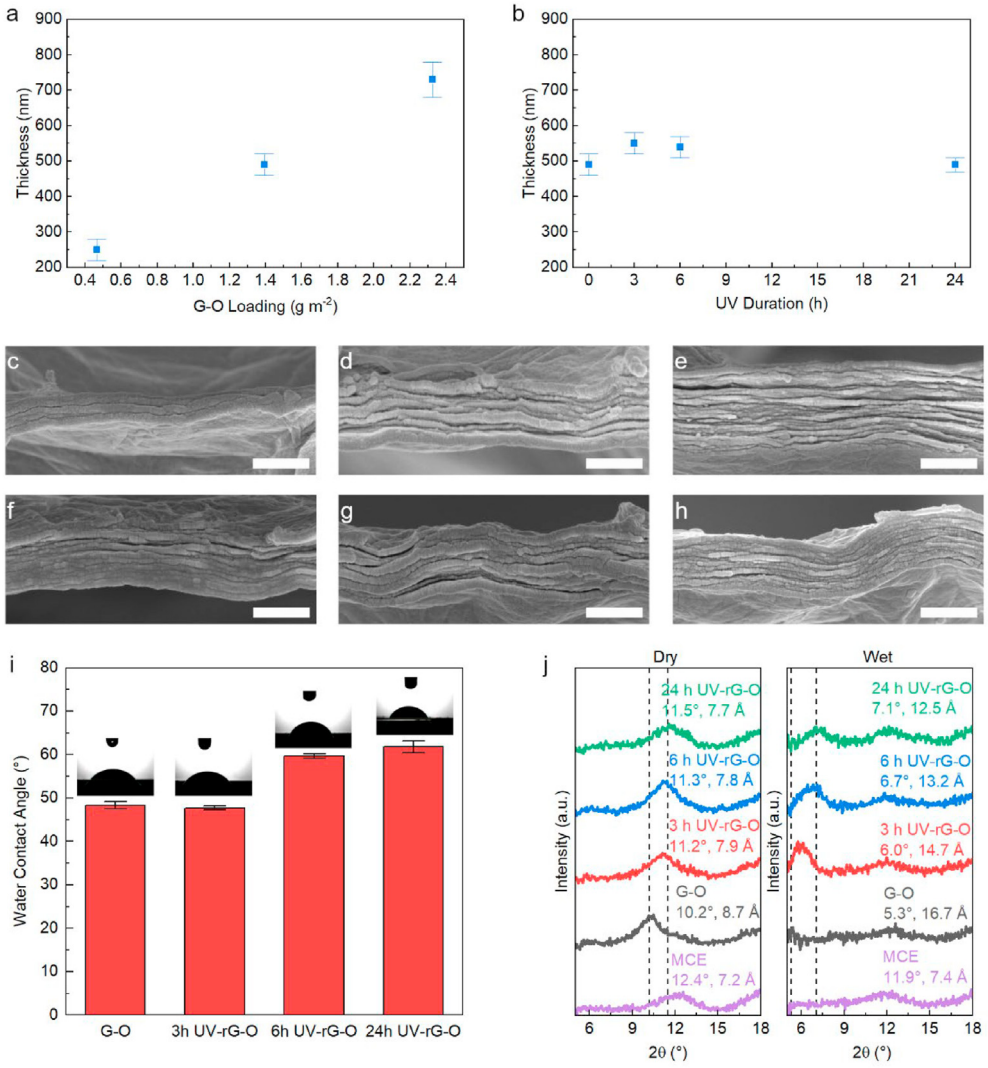

Fig. 1. Thickness of membranes from SEM images for a) G-O membranes with different loadings and b) different UV durations for UV-rG-O membranes. Error bars indicate one standard deviation. Corresponding SEM cross sections are c) 1, d) 3 and e) 5 mL G-O and f) 3 h, g) 6 h and h) 24 h UV-rG-O membranes as marked. Scale bars, 500 nm. i) Water contact angle measurements of 3 mL G-O on an MCE substrate that have been reduced using 0, 3, 6 and 24 h of UV irradiation, where the error bars are for one standard deviation. j) The calculated d-spacing from XRD spectra of G-O and UV-rG-O membranes in laboratory conditions (dry) and after soaking in water for 1 h (wet).

11.4° after 3, 6 and 24 h of UV exposure, respectively. These peaks correspond to a decrease in d-spacing from 8.7 Å to 7.9 Å, 7.8 Å and 7.7 Å. The d-spacing becomes narrower with longer irradiation time. This can be attributed to the removal of oxygen functional groups between the G-O layers. Furthermore, the broadening of the peak for the UV exposed films suggests that the d-spacing becomes less uniform throughout the depth of the film. When these films were soaked in water for 1 h, the peaks all experienced a negative shift due to water entering the interlayer channels and causing the membrane to swell. In the case of the G-O film, the peak is located at 5.3° and corresponds to a d-spacing of 16.7 Å. After UV radiation, the peak shifted to the right, 6.0°, 6.7° and 7.1° for 3, 6 and 24 h UV exposure, respectively, corresponding to d-spacings of 14.7 Å, 13.2 Å and 12.5 Å. UV-rG-O films show a lesser degree of swelling after soaking in water, which is likely due to the removal of oxygen functional groups and increased hydrophobicity of the G-O layers.

The chemical composition of the exposed and unexposed side (attached to the MCE substrate) of G-O and UV-rG-O films were studied by XPS, with the full survey spectra given in Figs. S3a and b. The C/O atomic ratio of the exposed side shows an increase from 2.02 for 0 h, 2.17 for 3 h, 2.30 for 6 h to 2.65 after 24 h of UV exposure (Fig. 2a, blue). The plot shows a relatively linear increase in C/O atomic ratio with the duration of UV exposure. For the unexposed side, the C/O atomic ratio remains ~2.0 for G-O and UV-rG-O films (Fig. 2a, red), even after 24 h of UV irradiation. XPS results suggest that the unexposed side of the film was not reduced. High resolution XPS C1s of the G-O and UV-rG-O films are shown in Fig. 2b. The C1s spectrum of G-O could be deconvoluted into three peaks corresponding to the following bonds: C—C and/or C═C (284.8 eV), C—O (epoxy/hydroxyls, 286.9 eV) and C═O (carbonyl, 288.4 eV) [46]. Comparing the C1s spectra of the exposed side of G-O and UV-rG-O films, the C—O bond experiences a decrease in peak intensity while the C═O peak remains relatively unchanged. Similar to previous works, the results indicate UV irradiation is capable of breaking the C—O bonds in the epoxy and/or hydroxyl groups, leading to partial reduction of G-O [44,47]. On the unexposed side, the peaks remain akin to the exposed side of G-O, even after 24 h irradiation. This result points to the gradual reduction along the depth of the film by UV radiation.

ToF-SIMS depth profiling through the G-O and UV-rG-O films was used to further investigate the degree of reduction at different depths after UV exposure. The samples were prepared by transferring the detached films from their MCE substrates onto a silicon wafer with the reduced side facing down. ToF-SIMS tape containing Si, C and O was used for 0, 3 and 6 h UV-rG-O while 24 h UV-rG-O was directly deposited on the silicon wafer. The depth profiling was

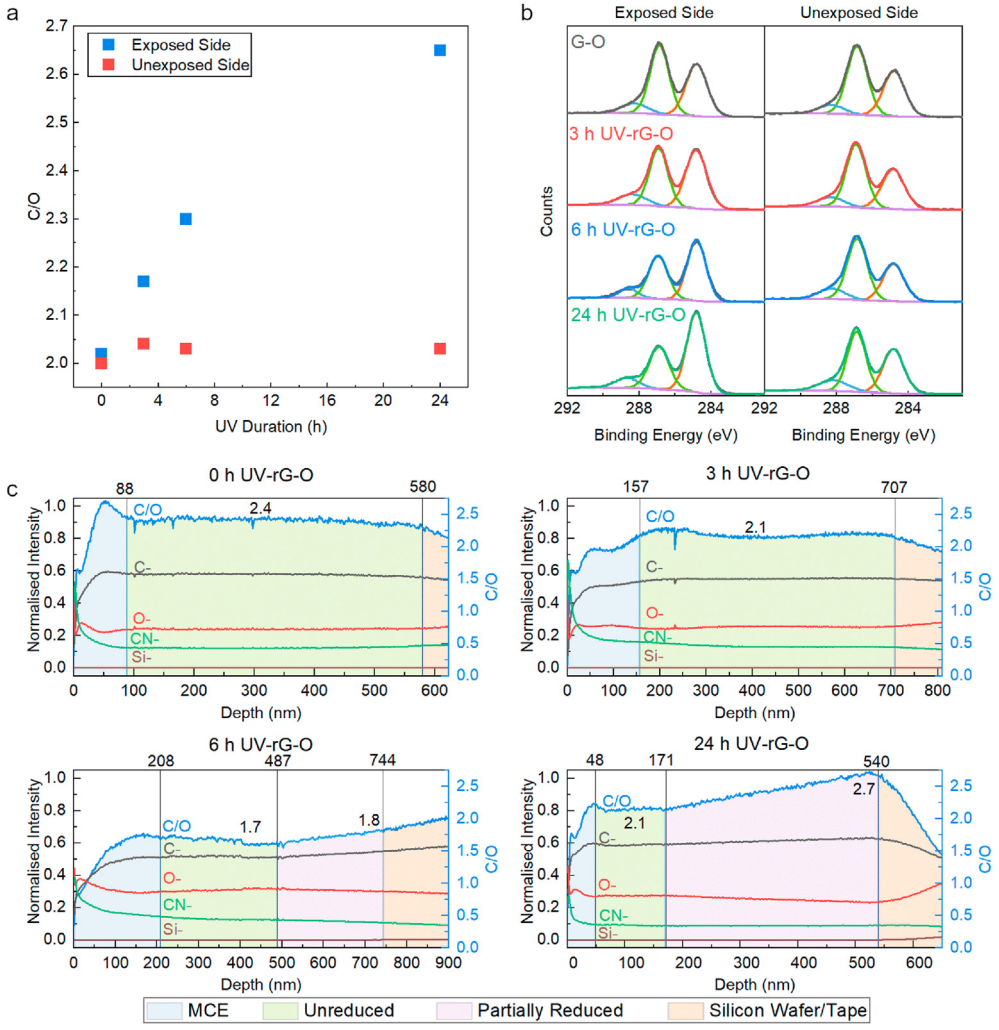

Fig. 2. a) C/O ratio of the top (exposed, blue) and bottom (green, previously attached to substrate) surface for G-O and UV-rG-O calculated from the atomic percentage obtained from the survey XPS. Their corresponding high resolution C1s spectra of both sides as shown in b). c) ToF-SIMS depth analysis of the C/O ratio for unreduced and UV-rG-O with the bottom side facing upwards when attached to a SiO_2/Si wafer.

conducted until the presence of silicon from the silicon wafer, or the ToF-SIMS tape was detected. The normalized ToF-SIMS depth profile is shown in Fig. 2c, where the C^-, O^-, CN^- and Si^- species are the grey, red, green, and brown curves, respectively. A C/O profile (blue curve) calculated from the ratio between the C^- and O^- species is also shown. The depth profiles consist of four regions: the MCE portion (blue) on the unreduced side of the film determined by the presence of CN^- species, whose intensity decreased and reached a constant, representing the end of the MCE region; the unreduced section of the film (green) showed a constant intensity of C^- and O^- species, and relatively stable C/O ratios; the partially reduced segment of the film (purple) experienced a decrease in O^- species, and an increase in the C/O ratio; the interface where the film meets the silicon tape or silicon wafer (orange) is indicated by the increase in Si^- species which is made clearer in Fig. S4.

The profile for the pristine G-O film has a constant C/O ratio throughout the entire depth of the film. Similarly, the 3 h UV-rG-O film also shows a relatively stable C/O ratio, likely due to the thin depth of reduction or little C/O ratio increase (2.2 from 2.1 for G-O indicated by XPS). The C/O ratio for 6 h UV-rG-O film increases from 1.7 to 1.8 across a depth of ~250 nm. This is also consistent with the XPS result where the C/O ratio increases slightly. By further increasing the UV exposure duration to 24 h, the depth of reduction increased to ~370 nm with the C/O ratio increasing from 2.1 to 2.7. Details of the film thickness, sputtering time and depth of junctions are included in Table S1. Results from ToF-SIMS confirm that UV irradiation up to 24 h increases the degree of reduction linearly from the unreduced portion of the film to the reduced surface of the film.

Raman spectroscopy was carried out on both sides of the G-O and UV-rG-O films as shown in Fig. S3c and d. The two prominent peaks are the D (1349 cm^{-1}) and G bands (1602 cm^{-1}) which originate from the κ-point photos of A_{1g} symmetry and the first order scattering of the E_{2g} phonon of sp^2 C atoms, respectively [48]. The positions and relative intensities of the two peaks remain unchanged on both sides of the film, suggesting that the rG-O films remain highly disordered after UV irradiation. We note that the Raman penetration depth (~700 nm for a 532 nm laser) could exceed the thickness of the film, whereas XPS and ToF-SIMS suggest partial reduction only on the exposed surface of the rG-O films.

3.2. Membrane filtration performance

G-O and UV-rG-O membranes were kept attached to their MCE substrate for dead-end filtration with 1.0 bar pressure applied using N_2 gas. The permeance was calculated using Eq. (1) where the time was taken for 18.0 mL of the feed to permeate through the membrane. Permeance for G-O and UV-rG-O membranes are provided in Fig. 3a and c, respectively. For G-O membranes with different loadings, the permeance decreases at a decreasing rate with greater G-O loading (thickness), from 9.46 to 4.69, 1.15 and 0.874 L m^{-2} h^{-1} for membranes prepared from 1, 2, 3 and 5 mL of G-O solution. This result is expected given thicker G-O membranes have been reported to possess greater tortuosity and a longer path for water to travel through [49]. In the case of UV-rG-O membranes prepared from the same loading of G-O, longer durations of UV exposure resulted in a decrease in permeance. This can be assigned to the decrease in d-spacing caused by the mild surface reduction as evident in Fig. S5 which shows permeance linearly increasing with d-spacing.

The separation factors for the membranes were calculated using Eqs. (2) and (3) with the isotope ratios, D/H and $^{18}O/^{16}O$, of water samples from the feed and retentate after 18.0 mL permeated through the membrane. The separation factor for D (grey) and ^{18}O (blue) for G-O and UV-rG-O are shown in Fig. 3b and d, respectively. In our experiments, water loss attributed to evaporation was recorded, with larger volumes observed for membranes that had a smaller permeance. In control experiments, the water loss originated from inside the dead-end cell while the sealed off vessel for the permeate experienced negligible changes. As a result, controls and Rayleigh's equation for fractional distillation [38] using Horita et al.'s equation to calculate the fractionation factor [39] (see Supporting Information) were employed to examine that the separation is from the membrane and not due to the isotope effect associated with phase transition from liquid to vapor (vapor pressure isotope effect) [38,39]. The relative isotope ratio experienced by the controls agrees well with Rayleigh's fractionation. Fig. 4 shows that the increase in heavier isotopes is greater than that obtained from the controls and Rayleigh's fractionation, demonstrating that the G-O and UV-rG-O membranes are capable of enriching D and ^{18}O in natural water.

3.2.1. Effect of membrane thickness on isotope separation

The possible mechanisms behind liquid-phase pressure driven isotope separation can be elucidated from the slope of the linear regression formed by plotting δD against $\delta^{18}O$ for the permeate and retentate water samples (Fig. S6a-c). Depending on the mechanism (adsorption effect, molecular diffusion and/or vapor pressure effect), isotope fractionation affects D and ^{18}O unequally. In the case groundwater circulating through the hydrological cycle, fractionation caused by the vaporization and precipitation of water is reported to result in a slope ranging from 5 to 8, depending on temperature and humidity [50]. In our case, the slopes for 1, 3 and 5 mL G-O membranes are smaller, 1.5 ± 0.6, 2.5 ± 0.2 and 4.8 ± 0.5, respectively. This result suggests that for 1 mL and 3 mL G-O membranes, the isotope separation is predominantly contributed by a mixture of molecular diffusion and adsorption which are reported to result in a slope of 0.5 and 3, respectively, when there is no vaporization [50,51]. In the case of 5 mL G-O membrane, a greater portion of the isotope fractionation is caused by vapor phase change as a greater volume of water was evaporated, although molecular diffusion and adsorption are also likely to contribute.

To eliminate the effect of vapor phase change, the change in isotope ratio (Eq. (4)) caused by the membrane was obtained by subtracting the change in isotope ratio from the vapor pressure isotope effect (calculated using Rayleigh's fractionation). From Fig. 5a and b, D and ^{18}O isotope ratio increases with loading except for $^{18}O/^{16}O$ for 5 mL G-O membrane suggesting the separation mechanisms dominant in the 5 mL G-O membrane is less effective for ^{18}O compared to D. One potential reason is the dominating mechanism has changed from molecular diffusion to adsorption separation, as this mechanism is less effective for enriching ^{18}O compared to D. Molecular diffusion (also known as bulk water diffusion) is reportedly based on the intermolecular interactions and the difference in molecular mass between isotopic water [31,51], and occurs in the region between the nanochannels without interacting directly with G-O. For bulk water diffusion at 25.0 °C under 1.0 bar, the self-diffusion coefficient has been determined to be 2.275×10^{-9}, 2.276×10^{-9} and 2.296×10^{-9} m^2 s^{-1} for HOD, $H_2^{18}O$ and $H_2^{16}O$, respectively [52]. The bulk diffusivity of $H_2^{16}O$ is reported to be ~1.009 times greater than both HOD and $H_2^{18}O$. Previous studies reported that higher G-O loading can result in the aggregation of G-O stacks that can hinder the diffusion of water vapor by causing blockages and pore deformation, leading to a decrease in flux and rejection efficiency [26,53]. It is expected that the molecular diffusion mechanism is hindered as G-O loading increases (for the 5 mL G-O membrane), resulting in a decrease in the efficiency of ^{18}O enrichment when compared to D. This is most evident in the slope of the line

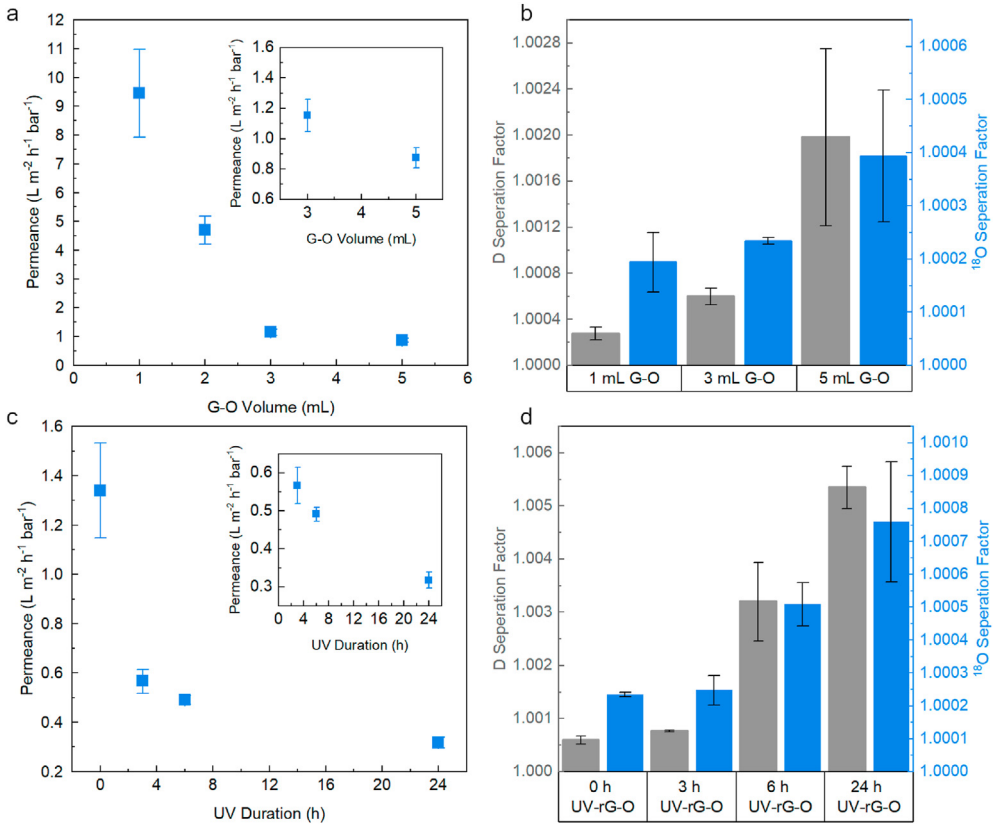

Fig. 3. a) Permeance and b) D and ^{18}O separation factors for G-O with different loadings. c) Permeance and d) D and ^{18}O separation factors for UV-rG-O with different UV durations. Error bars are one standard deviation of three individual experiments using a new membrane each time.

increasing from 1.5 to 4.8 as the loading increased from 1 mL to 5 mL of G-O solution, suggesting that molecular diffusion is no longer the dominant isotope fractionation effect.

The adsorption effect is reported to occur due to the difference in surface diffusion rates caused by the preference in adsorption and desorption interactions between the water isotopes and the oxygen functional groups on G-O (epoxy and hydroxyl groups) [8,14], and the lateral interactions with neighboring water molecules. In the hopping model, water molecules could migrate along the surface of G-O by hopping between energetically favorable adsorption sites if the water molecule has sufficient activation energy to overcome the energy barrier to jump to the neighboring site [30]. Water molecules form hydrogen bonds with the surface functional groups of G-O, where the difference in strength of the hydrogen bonds resulting from nuclear quantum effects is reported to give rise to selective adsorption and desorption [9]. The chemical affinity quantum sieving effect has been invoked to explain the differences in the preference between lighter and heavier isotopic molecules adsorbing. It has been reported that the only degree of freedom of adsorbed molecules is the vibrational energy normal to the surface which is influenced by the ZPE. The interaction is stronger for heavier isotopes that have lower ZPE, which allows them to have greater adsorption enthalpies and require higher energy to desorb [8]. Saidi et al., have modelled the hydrogen bonding formed between D_2O and H_2O with epoxy and hydroxyl groups, and found that the hydrogen bond formed with D is stronger for both groups [14]. Similarly, theoretical calculations performed by Krinkin show that $H_2^{18}O$ is less likely to rupture its hydrogen bond than $H_2^{16}O$ [32]. Coplen and Hanshaw have reported that the adsorption effect is likely to result in significantly greater D enrichment than ^{18}O enrichment [51]. As ZPE is related to the mass ratios of H/D and $^{16}O/^{18}O$, the difference in ZPE between $H_2^{16}O$ and $D_2^{16}O$ is larger than that between $H_2^{16}O$ and $H_2^{18}O$ due to the (much) larger change in mass ratio when substituting H with D compared to ^{16}O with ^{18}O [10]. As a result, the H/D substitution has a greater effect on the hydrogen bond environment [54]. The H/D and $^{16}O/^{18}O$ substitutions also affect the mass distribution of water molecules. Because $D_2^{16}O$ has twice the moment of inertia of $H_2^{16}O$ and $H_2^{18}O$ (resulting in a lower frequency of hindered rotation, and thus a lower ZPE and larger desorption activation energy for D_2O), a slower desorption rate than $H_2^{18}O$ is expected [12]. Therefore, $D_2^{16}O$ is expected to have the slowest surface diffusion rate followed by $H_2^{18}O$ and then $H_2^{16}O$ given the higher magnitude of isotope effect experienced by D-enriched water. We note that even though proton exchange to HDO may affect isotope effects, ZPE calculations for water molecules suggest D_2O has the lowest ZPE followed by HDO and then H_2O [55], and so the isotope separation mechanism should apply to the filtration process overall [14]. For membranes with higher G-O loading, the number of adsorption sites will increase, and as a result, the adsorption separation effect becomes more influential [51]. This is evident as D enrichment becomes significantly greater compared to ^{18}O enrichment for the 5 mL G-O membrane, whereas 3 mL G-O membrane is the most effective for ^{18}O enrichment due to the molecular diffusion effect.

3.2.2. *Effect of UV reduction on isotope separation*

Mild reduction with different UV durations altered the interlayer spacing and surface chemistry of G-O, which affect water diffusivity in confined nanochannels. The slope of the line for δD vs $\delta^{18}O$ values of the permeate and the retentate (Fig. S6b, d-f) increases from 2.5 ± 0.2, 3.1 ± 0.6, 6.2 ± 1.4 to 7.2 ± 1.5 for 0, 3, 6 and 24 h UV-rG-O membranes, respectively. With UV irradiation, the

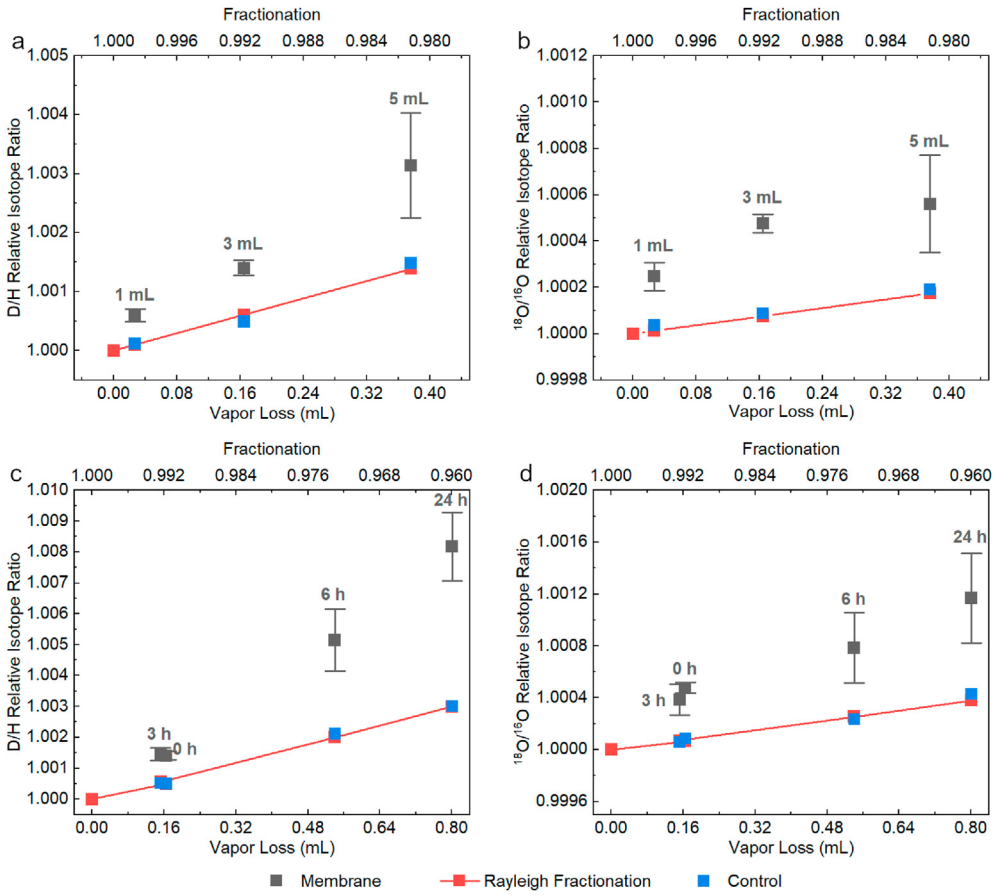

Fig. 4. Relative isotope ratio from membranes, control and Rayleigh's fractionation plotted against vapor loss during measurements for hydrogen and oxygen isotopes for G-O membranes prepared from different volumes, a) and b), and UV-rG-O membranes with different irradiation times c) and d). Error bars are one standard deviation of three individual experiments using a new membrane each time.

vapor pressure isotope effect plays a more dominant role in the isotope separation. Fig. 5c and d shows the change in isotope ratio from the membrane by subtracting the change caused by the vapor isotope effect. In the case of 3 h UV-rG-O, the change of $^{18}O/^{16}O$ remained similar to that of pristine G-O even though change of D/H increased, suggesting the adsorption effect that favors D separation from H is dominant. This shift to adsorption mechanism may be caused by the decrease of d-spacing from 16.7 Å to 14.7 Å. This results in thinner layers of water molecules inside the nano-channels, leading to a smaller portion experiencing bulk water diffusion. Additionally, Wen et al. reported that there are greater water molecule interactions with the oxygen functional groups [29], resulting in a greater portion undergoing surface diffusion. This is supported by the increase in both the change of D/H and $^{18}O/^{16}O$ for 6 h and 24 h UV-rG-O membranes, as their d-spacings after immersion are further decreased, 3.5 and 4.2 Å smaller than that of 3 mL G-O membranes, respectively.

Even though UV reduction partially removed oxygen functional groups and decreased the number of adsorption sites, there was no obvious decrease in heavy isotope enrichment. Previous studies by Saidi et al. reported that the content of oxygen functional groups does not affect the diffusivity of water molecules as long as there is a continuous film of water formed along the surface [14]. In liquid-phase permeation (dead-end filtration), a continuous film of water is expected to form in the nanochannels. These isotope separation results further support that the d-spacing, which is dependent on the swelling caused by the content of oxygen functional groups, is mainly responsible for enriching D and ^{18}O.

24 h UV-rG-O membrane shows the greatest isotopic enrichment of water, where the change in D/H (0.5%) and $^{18}O/^{16}O$ (0.08%) increased 8 and 2 times compared to those from G-O membranes, respectively. However, these values are much lower than those observed in other studies where vapor permeation or liquid-vapor permeation (e.g., air-gap membrane distillation and pervaporation) was used. In the literature, the highest D/H separation factor reportedly with G-O membranes was ~1.22 (88–95 °C) with vapor permeation [27]. In membrane distillation where the liquid to vapor interface occurs within the G-O membrane, the D/H separation factor reduced to 1.044–1.055 at 40 °C [28]. The significant decrease in separation factor was said by the authors to be owing to liquid water permeating through the membrane. A low $^{18}O/^{16}O$ separation factor of 1.0053 (60 °C) was reported with hydrophilic polymer membrane using pervaporation [55]. A coating of super-hydrophobic silica nanoparticles on G-O membrane reportedly achieved a D/H separation factor of 1.151 at 40 °C [29]. A $^{18}O/^{16}O$ separation factor (1.048 at 35 °C) was reported when hydrophobic poly(vinylidene fluoride) (PVDF) nanofibrous membranes were used in air-gap membrane distillation [18]. The lower separation factors have been reported as a result of condensed water molecules (liquid-phase) preventing Brownian motion and therefore limiting the effects of kinetic fractionation [14]. Additionally, air-gap membrane distillation and pervaporation have the benefit of vapor pressure isotope effect and Knudsen diffusion that synergistically combines with molecular diffusion and the adsorption effect, leading to greater D/H and $^{18}O/^{16}O$ separation factors, as reported in Ref. [15].

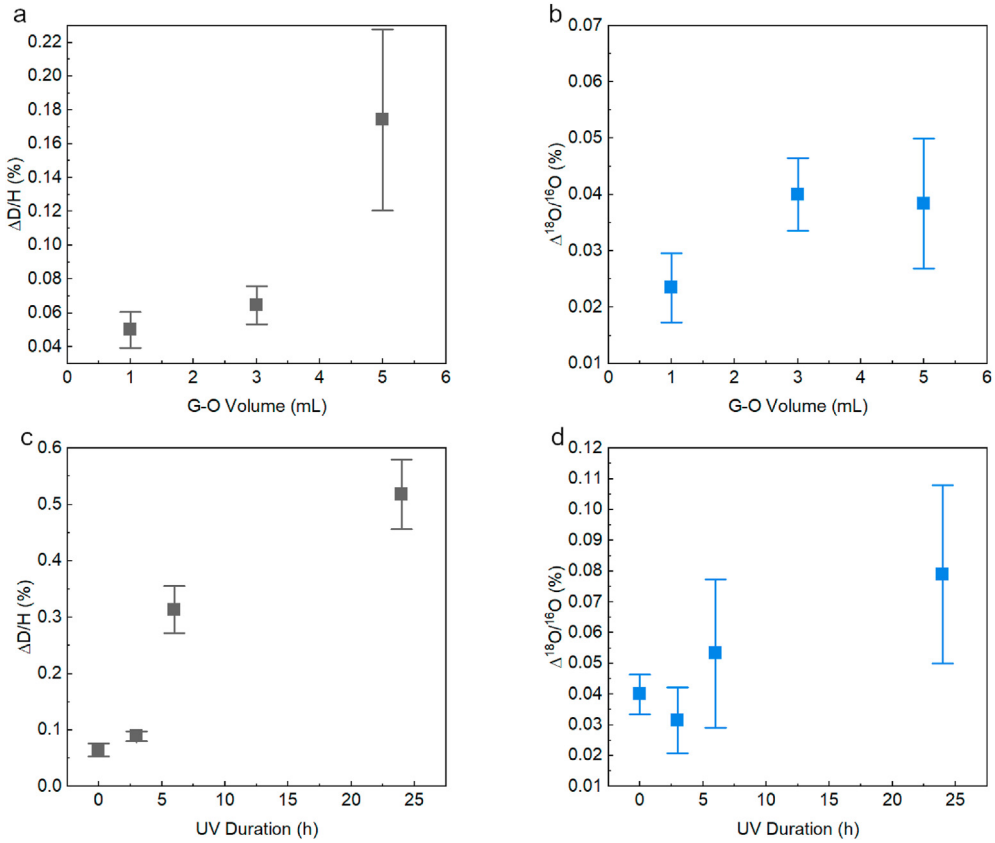

Fig. 5. Percentage increase in isotope ratio from the membrane by subtracting the enrichment from the vaporization effect. Effect of G-O loading on a) D/H increase and b) $^{18}O/^{16}O$ increase. Effect of different durations of UV reduction on c) D/H increase and d) $^{18}O/^{16}O$ increase. Error bars are one standard deviation of three individual experiments using a new membrane each time.

Even though isotope separation is significantly smaller in pressure-driven liquid-phase water isotope separation, the result from this study provides a better understanding of the mechanisms involved in graphene-based membranes which are otherwise difficult to isolate in vapor-phase membrane isotope separation. Further work focused on fabricating graphene-based membranes for vapor-phase membrane isotope separation can improve the separation factor for ^{18}O enrichment.

4. Conclusion

The separation of oxygen isotopic water has been demonstrated for the first-time using graphene-based membranes of different thicknesses and degrees of reduction with the use of dead-end filtration for liquid-phase isotope separation. D enrichment from H and ^{18}O enrichment from ^{16}O were achieved due to the differences in hydrogen bond strength with neighboring water molecules and oxygen functional groups on G-O, resulting in different rates of diffusion (molecular diffusion) and selective adsorption and desorption (adsorption effect). Heavier water isotopes were enriched in the retentate due to its slower diffusivity and were larger than the enrichment from water vapor loss. Our results showed increasing G-O thickness improved D/H and $^{18}O/^{16}O$ separation due to the increase in the number of adsorption sites. However, we observed a decrease in the efficiency of ^{18}O enrichment compared to D at higher G-O loading suggesting molecular diffusion has been hindered which may be owed to the aggregation of G-O stacks at higher G-O loading blocking diffusion. Results also showed UV-rG-O films experience increased heavier isotope separation with a higher D enrichment efficiency compared to ^{18}O, suggesting the adsorption mechanism is dominant which may be owing to the decrease in d-spacing from reduction, allowing greater water molecule interaction with the surface of G-O sheets. From the membranes tested, G-O membrane prepared from 3 mL of 0.5 mg mL^{-1} had the greatest $^{18}O/^{16}O$ percentage increase with further improvements in both D and ^{18}O enrichment achieved with 24 h UV reduction. From this study, the improvements can be attributed to the oxygen functional groups in G-O and UV-rG-O that act as adsorption sites, and the unique lamellar structure that has an easily adjustable d-spacing.

CRediT authorship contribution statement

Karin Ching: Writing – original draft, Conceptualization, Methodology, Validation, Formal analysis, Investigation, Visualization. **Andy Baker:** Writing – review & editing, Formal analysis, Methodology, Validation. **Ryoji Tanaka:** Writing – review & editing, Conceptualization, Methodology, Validation. **Tingwen Zhao:** Writing – review & editing, Investigation. **Zhen Su:** Writing – review & editing, Investigation. **Rodney S. Ruoff:** Writing – review & editing, Conceptualization, Methodology, Validation, Supervision. **Chuan Zhao:** Writing – review & editing, Resources, Supervision. **Xianjue Chen:** Writing – review & editing, Conceptualization, Methodology, Validation, Investigation, Resources, Supervision, Project administration, Funding acquisition.

Declaration of competing interest

The authors declare that they have no known competing financial interests or personal relationships that could have appeared to influence the work reported in this paper.

Acknowledgment

The authors thank the staff at the Mark Wainwright Analytical Centre at the University of New South Wales (UNSW) for access to analytical equipment. A special thanks to Songyan Yin and Bill Bin Gong for the assistance in ToF-SIMS depth profiling. X.C. acknowledges Australian Research Council DECRA (DE180100294), UNSW Science Faculty Research Grants Program and AMP Tomorrow Fund for funding support. C.Z. is grateful for the award of a Future Fellow from the Australian Research Council (FT170100224). R.S.R. acknowledges the support by the Institute for Basic Science (IBS-R019-D1).

Appendix A. Supplementary data

Supplementary data to this article can be found online at https://doi.org/10.1016/j.carbon.2021.10.009.

References

[1] O. Jacobson, D.O. Kiesewetter, X. Chen, Fluorine-18 radiochemistry, labeling strategies and synthetic routes, Bioconjugate Chem. 26 (1) (2015) 1–18, https://doi.org/10.1021/bc500475e.
[2] World Nuclear Association, Nuclear Power in the World Today (Last updated March 2021), https://www.world-nuclear.org/information-library/current-and-future-generation/nuclear-power-in-the-world-today.aspx.
[3] M. Markowska, A. Baker, M.S. Andersen, C.N. Jex, M.O. Cuthbert, G.C. Rau, P.W. Graham, H. Rutlidge, G. Mariethoz, C.E. Marjo, P.C. Treble, N. Edwards, Semi-arid zone caves: evaporation and hydrological controls on δ18O drip water composition and implications for speleothem paleoclimate reconstructions, Quat. Sci. Rev. 131 (2016) 285–301, https://doi.org/10.1016/j.quascirev.2015.10.024.
[4] Cambridge Isotope Laboratories, Inc., The Standard. https://www.isotope.com/corporate-overview/newsletters.cfm?nid=The%20Standard%20%E2%80%93%20July%202015&aid=CIL%20Isotope%20Separations%2C%20LLC%20%28CIS%29, July 2015. (Accessed 26 May 2021).
[5] T. Igarashi, T. Kambe, H. Kihara, Industrial separation of oxygen isotopes by oxygen distillation, J. Label. Compd. Radiopharm. 62 (12) (2019) 865–869, https://doi.org/10.1002/jlcr.3798.
[6] I. Dostrovsky, E.D. Hughes, D.R. Llewellyn, Fractional distillation and its application in the concentration of the heavy isotopes of oxygen and hydrogen, Nature 161 (4100) (1948) 858–859, https://doi.org/10.1038/161858a0.
[7] H.K. Rae, Selecting heavy water processes, Separat. Hydrogen Isotopes (1978) 1–26, https://doi.org/10.1021/bk-1978-0068.ch001.
[8] J.Y. Kim, H. Oh, H.R. Moon, Hydrogen isotope separation in confined nanospaces: carbons, zeolites, metal–organic frameworks, and covalent organic frameworks, Adv. Mater. 31 (20) (2019) 1805293, https://doi.org/10.1002/adma.201805293.
[9] A. Berger, G. Ciardi, D. Sidler, P. Hamm, A. Shalit, Impact of nuclear quantum effects on the structural inhomogeneity of liquid water, Proc. Natl. Acad. Sci. Unit. States Am. 116 (7) (2019) 2458–2463, https://doi.org/10.1073/pnas.1818182116.
[10] S. Scheiner, Calculation of isotope effects from first principles, Biochim. Biophys. Acta Bioenerg. 1458 (1) (2000) 28–42, https://doi.org/10.1016/S0005-2728(00)00058-X.
[11] R. Mills, K.R. Harris, The effect of isotopic substitution on diffusion in liquids, Chem. Soc. Rev. 5 (1976) 215–231, https://doi.org/10.1039/CS9760500215, 0.
[12] J.A. Smith, F.E. Livingston, S.M. George, Isothermal desorption kinetics of crystalline H2O, H218O, and D2O ice multilayers, J. Phys. Chem. B 107 (16) (2003) 3871–3877, https://doi.org/10.1021/jp022503s.
[13] A.G. Chmielewski, G. Zakrzewska-Trznadel, N.R. Miljevic, W.A. van Hook, Investigation of the separation factor between light and heavy water in the liquid/vapor membrane permeation process, J. Membr. Sci. 55 (3) (1991) 257–262, https://doi.org/10.1016/S0376-7388(00)80580-3.
[14] P. Saidi, L.K. Béland, M.R. Daymond, Graphene oxide membranes for water isotope filtration: insight at the nano- and microscale, J. Phys. Chem. C 124 (49) (2020) 26864–26873, https://doi.org/10.1021/acs.jpcc.0c08817.
[15] G. Zakrzewska-Trznadel, A.G. Chmielewski, N.R. Miljević, Separation of protium/deuterium and oxygen-16/oxygen-18 by membrane distillation, J. Membr. Sci. 113 (2) (1996) 337–342, https://doi.org/10.1016/0376-7388(95)00131-X.
[16] J. Kim, S.E. Park, T.-S. Kim, D.-Y. Jeong, K.-H. Ko, Isotopic water separation using AGMD and VEMD, Nukleonika 49 (4) (2004) 137–142. Retrieved from, http://www.nukleonika.pl/.
[17] J. Kim, D.-S. Chang, Y.-Y. Choi, Separation of oxygen isotopic water by using a pressure-driven air gap membrane distillation, Ind. Eng. Chem. Res. 48 (11) (2009) 5431–5438, https://doi.org/10.1021/ie900277r.
[18] R. Moradi, J. Karimi-Sabet, M. Shariaty-Niassar, Y. Amini, Air gap membrane distillation for enrichment of H218O isotopomers in natural water using poly(vinylidene fluoride) nanofibrous membrane, Chem. Eng. Process: Process Intensif. 100 (2016) 26–36, https://doi.org/10.1016/j.cep.2015.11.015.
[19] M. Lozada-Hidalgo, S. Zhang, S. Hu, A. Esfandiar, I.V. Grigorieva, A.K. Geim, Scalable and efficient separation of hydrogen isotopes using graphene-based electrochemical pumping, Nat. Commun. 8 (1) (2017) 15215, https://doi.org/10.1038/ncomms15215.
[20] S. Hu, K. Gopinadhan, A. Rakowski, M. Neek-Amal, T. Heine, I.V. Grigorieva, S.J. Haigh, F.M. Peeters, A.K. Geim, M. Lozada-Hidalgo, Transport of hydrogen isotopes through interlayer spacing in van der Waals crystals, Nat. Nanotechnol. 13 (6) (2018) 468–472, https://doi.org/10.1038/s41565-018-0088-0.
[21] S.K. Ujjain, A. Bagusetty, Y. Matsuda, H. Tanaka, P. Ahuja, C. de Tomas, M. Sakai, F. Vallejos-Burgos, R. Futamura, I. Suarez-Martinez, M. Matsukata, A. Kodama, G. Garberoglio, Y. Gogotsi, J. Karl Johnson, K. Kaneko, Adsorption separation of heavier isotope gases in subnanometer carbon pores, Nat. Commun. 12 (1) (2021) 546, https://doi.org/10.1038/s41467-020-20744-6.
[22] H.P. Boehm, A. Clauss, U. Hofmann, Graphite oxide and its membrane properties, J. Chim. Phys. 58 (1961) 141–147, https://doi.org/10.1051/jcp/1961580141.
[23] R.R. Nair, H.A. Wu, P.N. Jayaram, I.V. Grigorieva, A.K. Geim, Unimpeded permeation of water through helium-leak–tight graphene-based membranes, Science 335 (6067) (2012) 442, https://doi.org/10.1126/science.1211694.
[24] M. Zhang, K. Guan, Y. Ji, G. Liu, W. Jin, N. Xu, Controllable ion transport by surface-charged graphene oxide membrane, Nat. Commun. 10 (1) (2019) 1253, https://doi.org/10.1038/s41467-019-09286-8.
[25] K. Huang, G. Liu, Y. Lou, Z. Dong, J. Shen, W. Jin, A graphene oxide membrane with highly selective molecular separation of aqueous organic solution, Angew. Chem. 53 (27) (2014) 6929–6932, https://doi.org/10.1002/anie.201401061.
[26] A. Mohammadi, M.R. Daymond, A. Docoslis, Graphene oxide membranes for isotopic water mixture filtration: preparation, physicochemical characterization, and performance assessment, ACS Appl. Mater. Interfaces 12 (31) (2020) 34736–34745, https://doi.org/10.1021/acsami.0c04122.
[27] G.J. Sevigny, R.K. Motkuri, D.W. Gotthold, L.S. Fifield, A.P. Frost, W. Bratton, Separation of Titrated Water Using Graphene Oxide, PNNL-24411 AF5805010, Pacific Northwest National Laboratory (PNNL), Richland, WA (United States), 2015.
[28] M. Wen, M. Chen, G.-K. Ren, P.-L. Li, C. Lv, Y. Yao, Y.-K. Liu, S.-J. Deng, Z. Zheng, C.-G. Xu, D.-L. Luo, Enhancing the selectivity of hydrogen isotopic water in membrane distillation by using graphene oxide, J. Membr. Sci. (2020), https://doi.org/10.1016/j.memsci.2020.118237.
[29] M. Wen, M. Chen, K. Chen, P.-L. Li, C. Lv, X. Zhang, Y. Yao, W. Yang, G. Huang, G.-K. Ren, S.-J. Deng, Y.-K. Liu, Z. Zheng, C.-G. Xu, D.-L. Luo, Superhydrophobic composite graphene oxide membrane coated with fluorinated silica nanoparticles for hydrogen isotopic water separation in membrane distillation, J. Membr. Sci. 626 (2021) 119136, https://doi.org/10.1016/j.memsci.2021.119136.
[30] I. Medveď, R. Černý, Surface diffusion in porous media: a critical review, Microporous Mesoporous Mater. 142 (2) (2011) 405–422, https://doi.org/10.1016/j.micromeso.2011.01.015.
[31] H. Pinto de Magalhães, M.S. Brennwald, R. Kipfer, Diverging effects of isotopic fractionation upon molecular diffusion of noble gases in water: mechanistic insights through ab initio molecular dynamics simulations, Environ. Sci.: Process. Impacts. 19 (3) (2017) 405–413, https://doi.org/10.1039/C6EM00614K.
[32] D. Krinkin, Anomalously large kinetic isotope effect, Cent. Eur. J. Chem. 5 (4) (2007) 1019–1063, https://doi.org/10.2478/s11532-007-0048-2.
[33] A.J. Fletcher, K.M. Thomas, Kinetic isotope quantum effects in the adsorption of H2O and D2O on porous carbons, J. Phys. Chem. C 111 (5) (2007) 2107–2115, https://doi.org/10.1021/jp065105o.
[34] D.-D. Han, Y.-L. Zhang, Y. Liu, Y.-Q. Liu, H.-B. Jiang, B. Han, X.-Y. Fu, H. Ding, H.-L. Xu, H.-B. Sun, Bioinspired graphene actuators prepared by unilateral UV irradiation of graphene oxide papers, Adv. Funct. Mater. 25 (28) (2015) 4548–4557, https://doi.org/10.1002/adfm.201501511.
[35] H. Yu, Y. He, G. Xiao, Y. Fan, J. Ma, Y. Gao, R. Hou, J. Chen, Weak-reduction graphene oxide membrane for improving water purification performance, J. Mater. Sci. Technol. 39 (2020) 106–112, https://doi.org/10.1016/j.jmst.2019.08.024.
[36] W.S. Hummers, R.E. Offeman, Preparation of graphitic oxide, J. Am. Chem. Soc. 80 (6) (1958) 1339, https://doi.org/10.1021/ja01539a017.
[37] N.I. Kovtyukhova, P.J. Ollivier, B.R. Martin, T.E. Mallouk, S.A. Chizhik, E.V. Buzaneva, A.D. Gorchinskiy, Layer-by-Layer assembly of ultrathin composite films from micron-sized graphite oxide sheets and polycations, Chem. Mater. 11 (3) (1999) 771–778, https://doi.org/10.1021/cm981085u.
[38] L. Rayleigh, LIX. On the distillation of binary mixtures, Philos. Mag. A 4 (23) (1902) 521–537, https://doi.org/10.1080/14786440209462876.
[39] J. Horita, D.J. Wesolowski, Liquid-vapor fractionation of oxygen and hydrogen

isotopes of water from the freezing to the critical temperature, Geochem. Cosmochim. Acta 58 (16) (1994) 3425–3437, https://doi.org/10.1016/0016-7037(94)90096-5.
[40] International Atomic Energy Agency, Reference Sheet for International Measurement Standards, 2006. Issued date: December.
[41] W.C. Duer, G.L. Bertrand, Apparent heat of formation of HDO in mixtures of H2O and D2O, J. Chem. Phys. 53 (8) (1970) 3020–3022, https://doi.org/10.1063/1.1674442.
[42] I. Litvak, Y. Anker, H. Cohen, On-line in situ determination of deuterium content in water via FTIR spectroscopy, RSC Adv. 8 (50) (2018) 28472–28479, https://doi.org/10.1039/C8RA03312A.
[43] V.A. Smirnov, N.N. Denisov, M.V. Alfimov, Photochemical reduction of graphite oxide, Nanotechnol Russ 8 (1) (2013) 1–22, https://doi.org/10.1134/S1995078013010151.
[44] Y. Matsumoto, M. Koinuma, S.Y. Kim, Y. Watanabe, T. Taniguchi, K. Hatakeyama, H. Tateishi, S. Ida, Simple photoreduction of graphene oxide nanosheet under mild conditions, ACS Appl. Mater. Interfaces 2 (12) (2010) 3461–3466, https://doi.org/10.1021/am100900q.
[45] M. Shams, L.M. Guiney, L. Huang, M. Ramesh, X. Yang, M.C. Hersam, I. Chowdhury, Influence of functional groups on the degradation of graphene oxide nanomaterials, Environ. Sci.: Nano 6 (7) (2019) 2203–2214, https://doi.org/10.1039/C9EN00355J.
[46] D.C. Marcano, D.V. Kosynkin, J.M. Berlin, A. Sinitskii, Z. Sun, A. Slesarev, L.B. Alemany, W. Lu, J.M. Tour, Improved synthesis of graphene oxide, ACS Nano 4 (8) (2010) 4806–4814, https://doi.org/10.1021/nn1006368.
[47] P. Sun, Q. Chen, X. Li, H. Liu, K. Wang, M. Zhong, J. Wei, D. Wu, R. Ma, T. Sasaki, H. Zhu, Highly efficient quasi-static water desalination using monolayer graphene oxide/titania hybrid laminates, NPG Asia Mater. 7 (2) (2015) e162, https://doi.org/10.1038/am.2015.7.
[48] S. Stankovich, D.A. Dikin, R.D. Piner, K.A. Kohlhaas, A. Kleinhammes, Y. Jia, Y. Wu, S.T. Nguyen, R.S. Ruoff, Synthesis of graphene-based nanosheets via chemical reduction of exfoliated graphite oxide, Carbon 45 (7) (2007) 1558–1565, https://doi.org/10.1016/j.carbon.2007.02.034.
[49] Y. You, X.H. Jin, X.Y. Wen, V. Sahajwalla, V. Chen, H. Bustamante, R.K. Joshi, Application of graphene oxide membranes for removal of natural organic matter from water, Carbon 129 (2018) 415–419, https://doi.org/10.1016/j.carbon.2017.12.032.
[50] D.L. Graf, I. Friedman, W.F. Meents, The Origin of Saline Formation Waters, II: Isotopic Fractionation by Shale Micropore Systems, Circular No, 1965, p. 393. Retrieved from, http://hdl.handle.net/2142/44611.
[51] T.B. Coplen, B.B. Hanshaw, Ultrafiltration by a compacted clay membrane—I. Oxygen and hydrogen isotopic fractionation, Geochem. Cosmochim. Acta 37 (10) (1973) 2295–2310, https://doi.org/10.1016/0016-7037(73)90105-1.
[52] A.J. Easteal, A.V.J. Edge, L.A. Woolf, Isotope effects in water. Tracer diffusion coefficients for water(oxygen-18) (H218O) in ordinary water, J. Phys. Chem. 88 (24) (1984) 6060–6063, https://doi.org/10.1021/j150668a065.
[53] J. Shen, G. Liu, K. Huang, W. Jin, K.-R. Lee, N. Xu, Membranes with fast and selective gas-transport channels of laminar graphene oxide for efficient CO2 capture, Angew. Chem. Int. Ed. 54 (2) (2015) 578–582, https://doi.org/10.1002/anie.201409563.
[54] Y. Lin, J. Horita, O. Abe, Adsorption isotope effects of water on mesoporous silica and alumina with implications for the land-vegetation-atmosphere system, Geochem. Cosmochim. Acta 223 (2018) 520–536, https://doi.org/10.1016/j.gca.2017.12.021.
[55] J.R. Hulston, Revised zero-point energy calculation for H2O+D2O⇋2HDO isotopic equilibrium, J. Chem. Phys. 50 (3) (1969) 1483–1484, https://doi.org/10.1063/1.1671222.